Available online at www.sciencedirect.com
ScienceDirect
Journal of Power Sources 161 (2006) 1161–1168
JOURNAL OF POWER SOURCES
www.elsevier.com/locate/jpowsour

Transient behavior of a PEMFC

Shih-Ming Chang, Hsin-Sen Chu *

Department of Mechanical Engineering, National Chiao Tung University, Hsinchu, Taiwan 300, Taiwan

Received 8 March 2006; received in revised form 8 June 2006; accepted 8 June 2006
Available online 14 August 2006

Abstract

The transient behavior of a proton exchange membrane fuel cell (PEMFC) with porosity is investigated in this study using a two-phase, half-cell model. The thin film agglomerate approach is used to model the catalyst layer. Both vapor transport and liquid water transport in the PEMFC are examined in this study. Proton transport is much faster than the gaseous and liquid water transport. The ionic potential reaches a steady state level in $\sim 10^{-1}$ s but liquid water transport takes ~10 s. The variation of the ionic potential loss reaches a critical value, decreasing to a steady state, and is not monotonic. The gas diffusion layer (GDL) and the catalyst layer (CL) porosity, which can affect cell performance, have been carefully investigated. The current density rises rapidly within 10^{-2} s, then remaining constant. After 1 s, this is affected by the cell voltage, GDL porosity, and CL porosity, and if the GDL porosity is below 0.4, the current density drops. For the gas diffusion layer porosity, the current density increases between $\varepsilon_{GDL} = 0.2$ and $\varepsilon_{GDL} = 0.5$, with increased GDL porosity. For the catalyst layer porosity, the optimum value appears between $\varepsilon_{CL} = 0.06$ and $\varepsilon_{CL} = 0.1$.

Keywords: PEMFC; Transient analysis; Two-phase; Thin film-agglomerate model; Porosity

1. Introduction

In recent years, fuel cells have been actively developed for use in portable devices including mobile phones, computer notebooks, power tools, digital cameras, etc., proton exchange membrane (PEM) fuel cells have many advantages, such as a potentially lower cost per kW, fast start-up, and a lower operating temperature. These applications require a highly dynamic model, but most recent fuel cell studies use steady state, rather than transient models. Developing a transient model, for obtaining higher PEM fuel cell performance is therefore very important.

A PEMFC is a sandwich-like structure consisting of a membrane, gas diffusion layers (GDL), and catalyst layers (CL). The catalyst layer is more complex than the other layers, because it is here that electrochemical reactions take place, and different phase types are present. There are many approaches for studying the catalyst layer. If it is considered to be an interface [1–3], many parameters will be ignored, and the results will be inaccurate. Generally speaking, the results will be higher than they should be. Various approaches have been proposed to counter this, such as the thin film model [4] and agglomerate model [5–10]. In the thin-film model, catalyst particles are covered by a polymer electrolyte film, and gas pores exist only within the electrode. Film thickness is uniform and very small compared to pore size. In the agglomerate model, catalyst particles, electrolytes, and gas pores form a homogeneous mixture. Several researchers [11–14] compared their model to experimental data. Broka and Ekdunge [11] have suggested that the agglomerate model is more accurate relative to other models.

Most models treat the catalyst layer as a single phase. It is in fact, multiphase in a fuel cell. More sophisticated treatments have been used for a two-phase flow in fuel cells [15–19]. Van Nguyen and co-workers [16–19] assumed that liquid water transport through the porous electrode is driven by gas flow shear and capillary forces, and they also assumed a net flux through the membrane. Permeability was taken to be a linear saturation level function. According to the two-phase model, if liquid water is neglected, the cell performance will be overestimated. Portable device applications require highly dynamic loadings so PEMFC steady state models must have some imperfections. Most studies take a single factor into consideration, leading to overestimations.

A transient, two-phase, one-dimensional, isothermal and isobaric model of a proton exchange membrane fuel cell cathode is the basis for this study. The approach offered by Springer et al. [3,20] is assumed for the membrane. The thin

* Corresponding author. Tel.: +886 3 571 2121x55115; fax: +886 3 572 7930.
E-mail address: hschu@cc.nctu.edu.tw (H.-S. Chu).

0378-7753/$ – see front matter © 2006 Elsevier B.V. All rights reserved.
doi:10.1016/j.jpowsour.2006.06.025

Nomenclature

a	surface area per unit volume
b	tafel slope
C_j	concentration of species j (mol cm^{-3})
D_j	diffusion coefficient of species j (cm^2 s^{-1})
F	Faraday constant
H	Henry constant (atm cm^3 mol^{-1})
i	current density (A cm^{-2})
k_T	oxygen reaction rate constant (s^{-1})
k_c	condensation rate
k_v	evaporation rate
K	permeability (cm^2)
M	molecular weight
N_j	molar flux of species j (mol cm^{-2} s^{-1})
P	pressure (atm)
r	radius (cm)
s	liquid water saturation level in porous medium
T	temperature (K)
V_s	cell potential (V)
y	mole fraction

Greek

δ	thickness (cm)
ε	porosity or volumetric fraction
ϕ	ionic potential (V)
φ	Thiele modulus
κ	conductivity (Ω^{-1} cm^{-1})
λ	water content
μ	viscosity (g cm^{-1} s^{-1})
ρ	density (g cm^{-3})
τ	tortuosity
ξ	effectiveness factor

Subscripts and superscripts

agg	agglomerate
CL	catalyst layer
eff	effective
g	gas phase
GDL	gas diffusion layer
MEM	membrane
N	Nafion phase
O_2	oxygen
p	proton
Pt	platinum
sat	saturation
v	vapor water
w	liquid water

film-agglomerate approach presented by Lin et al. [19] is applied to describe the catalyst layer. In terms of modeling two-phase transport in both the gas diffusion layer and catalyst layer, the approach developed by Natarajan and Van Nguyen [18] is applied. Presenting interactions between each parameter and the cell performance in the transient state, such as gas diffusion layer porosity and catalyst layer porosity, is the objective of this study. It is hoped that appropriate parameters will help generate a higher performance fuel cell.

2. Mathematical modeling

This study is based on the model of Lin et al. [19] to develop a half-cell transient model (Fig. 1) and investigates how the GDL and CL porosities affect the fuel cell performance. It also analyzes electrochemical kinetics and transport of oxygen, vapor water, and liquid water in the GDL, the catalyst layer, and in the proton exchange membrane. After PEMFC start-up, air diffuses from the channel to the catalyst layer via the gas diffusion layer. In the meantime, oxygen dissolves into the Nafion film and reaches the pellet surface; then liquid water is generated. The following assumptions are made:

(1) The gas phase obeys the ideal gas law.
(2) In the GDL and CL, electronic resistance is negligible.
(3) Catalyst pellets are treated as cylindrical and consist of carbon-supported platinum and Nafion, covered by a Nafion film.
(4) Catalyst pellet radius and Nafion film thickness are uniform in the catalyst layer.
(5) Catalyst pellets are treated as homogeneous and oxygen diffuses into pellets via Nafion film.
(6) The Thiele modulus approach is applied.
(7) The oxygen reduction reaction generates liquid phase water.
(8) The ionic potential between the anode catalyst layer and the membrane is approximately zero because of the fast hydrogen oxidation reaction rate.

Conservation equations are listed in Table 1 with five variables.

(1) The concentration of oxygen in the gas phase [$C^g_{O_2}$].
(2) The concentration of vapor water in the gas phase [C^g_v].
(3) The liquid water saturation level [s] (the ratio between liquid water volume and total void volume in the porous medium).
(4) The concentration of liquid water in Nafion phase [C^N_w].
(5) The ionic potential [ϕ] (potential in Nafion phase).

The flux expression of gas phase is

$$N_j = -D_j[\varepsilon_0^i(1-s)]^\tau \nabla C_j^g \quad (1)$$

ε_0^i is intrinsic porosity of GDL or CL. With diffusion coefficient, D_j, nothing but temperature dependence is considered [21]. The Bruggeman correlation is used to assess porosity and tortuosity effects.

Water interfacial transfer rate between liquid and vapor, R_w, is the same as that used by Lin et al. [19]. R_{O_2} is the reaction rate of oxygen in the catalyst layer.

$$R_{O_2} = \frac{RT/H^N_{O_2}}{(\delta_N/a_r D^N_{O_2}) + (\delta_w/a_r D^w_{O_2})(H^w_{O_2}/H^N_{O_2}) + (1/\xi k_T)} C^g_{O_2} \quad (2)$$

$H^N_{O_2}$ and $H^w_{O_2}$ are the Henry's constants. $H^N_{O_2}$ is the oxygen between air and the Nafion phase and $H^w_{O_2}$ is the oxygen between

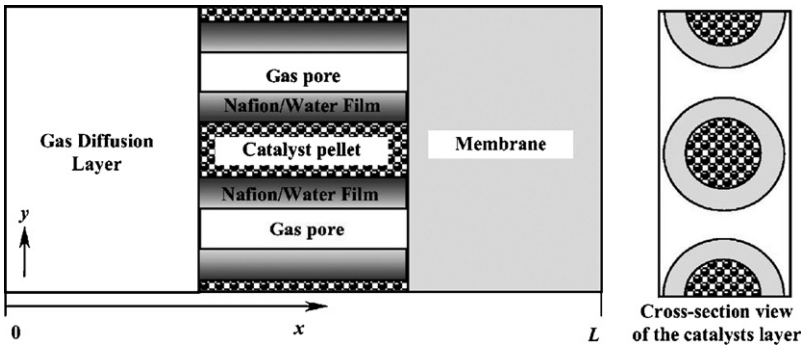

Fig. 1. Schematic of the model domain [19].

air and liquid water. δ_N is the thickness of the Nafion film. $D^N_{O_2}$ is the diffusivity of oxygen in the Nafion, and $D^w_{O_2}$ is the diffusivity of oxygen in liquid water. a_r is the outer surface area of agglomerates per catalyst layer unit volume.

$$a_r = \frac{2}{r_{Agg} + \delta_N}(1 - \varepsilon_0^{CL}) \tag{3}$$

r_{Agg} is the radius of a catalyst pellet. Liquid water forms a film around the top of Nafion film. If it is not evaporated, its thickness can be estimated by

$$\delta_w = \frac{\varepsilon_0^{CL} s}{a_r} \tag{4}$$

The reaction rate constant

$$k_T = (1 - \varepsilon_0^{CL}) \frac{1}{4FC_{O_2,eff}} a_{Pt}^{agg} i_0 \exp\left[-\frac{2.303(V_s - \phi - U_{ref})}{b}\right] \tag{5}$$

The active catalyst surface area per unit volume of agglomerates

$$a_{Pt}^{agg} = \frac{a_{Pt} m_{Pt}}{\delta_{CL}(1 - \varepsilon_0^{CL})} \tag{6}$$

a_{Pt} is the surface area per mass. m_{Pt} is the catalyst loading of the electrode. δ_{CL} is the thickness of catalyst layer and b is the Tafel slope.

Table 1
Governing equation

Variables	GDL	CL	MEM
$C^g_{O_2}$	$\frac{\partial}{\partial t}((1-s)\varepsilon_0^{GDL} C^g_{O_2}) = D_{O_2}\varepsilon_0^{GDL^\tau}[[(1-s)]^\tau \nabla^2 C^g_{O_2} + \nabla[(1-s)]^\tau \nabla C^g_{O_2}]$	$\frac{\partial}{\partial t}((1-s)\varepsilon_0^{CL} C^g_{O_2}) = -R_{O_2} + D_{O_2}\varepsilon_0^{CL^\tau}[[(1-s)]^\tau \nabla^2 C^g_{O_2} + \nabla[(1-s)]^\tau \nabla C^g_{O_2}]$	$C^g_{O_2} = 0$
C^g_v	$\frac{\partial}{\partial t}((1-s)\varepsilon_0^{GDL} C^g_v) = -R_w + D_v\varepsilon_0^{GDL^\tau}[[(1-s)]^\tau \nabla^2 C^g_v + \nabla[(1-s)]^\tau \nabla C^g_v]$	$\frac{\partial}{\partial t}((1-s)\varepsilon_0^{CL} C^g_v) = -R_w + D_v\varepsilon_0^{CL^\tau}[[(1-s)]^\tau \nabla^2 C^g_v + \nabla[(1-s)]^\tau \nabla C^g_v]$	$C^g_v = 0$
s	$\frac{\varepsilon_0^{GDL}\rho_w}{M_w}\frac{\partial s}{\partial t} = \frac{\rho_w K_{w,0}}{M_w \mu_w}\left(-\frac{dp_c}{ds}\right)(s\nabla^2 s + (\nabla s)^2) + R_w$	$\frac{\varepsilon_0^{CL}\rho_w}{M_w}\frac{\partial s}{\partial t} = (4n_d^{CL} + 2)R_{O_2} + R_w + \frac{\rho_w K_{w,0}}{M_w \mu_w}\left(-\frac{dp_c}{ds}\right)(s\nabla^2 s + (\nabla s)^2)$	$s = 0$
C^N_w	$\varepsilon_m^{GDL}\frac{\partial C^N_w}{\partial t} = D^N_w \nabla^2 C^N_w$	$\varepsilon_m^{CL}\frac{\partial C^N_w}{\partial t} = D^N_w \nabla^2 C^N_w$	$\varepsilon_m \frac{\partial C^N_w}{\partial t} = D^N_w \nabla^2 C^N_w + \frac{n_d \kappa_N}{F}\nabla^2 V_+$
ϕ		$\kappa_{N,eff}\nabla^2\phi - 4FR_{O_2} = 0$	$\nabla^2\phi = 0$

Table 2
Boundary conditions

Variables	$X = 0$	GDL/CL	CL/MEM	$X = L$
$C^g_{O_2}$	$C^g_{O_2} = C^{air}_{O_2}$	$N^g_{O_2}\|_{GDL} = N^g_{O_2}\|_{GDL}$	$N^g_{O_2}\|_{CL} = 0$	$C^g_{O_2} = 0$
C^g_v	$C^g_v = C^{air}_v$	$N^g_v\|_{GDL} = N^g_v\|_{GDL}$	$N^g_v\|_{CL} = 0$	$C^g_{O_2} = 0$
s	$s = 0$	$N_w\|_{GDL} = N_w\|_{GDL}$	$N_w\|_{CL} = 0$	$s = 0$
C^N_w	$C^N_w = 0$	$N^N_w\|_{GDL} = N^N_w\|_{GDL}$	$N^N_w\|_{CL} = N^N_w\|_{CL}$	$C^N_w\|_{MEM} = C^{N,eq}_{w(anode)}$
ϕ	–	$i_p\|_{GDL} = 0$	$i_p\|_{CL} = i_p\|_{CL}$	$\phi = 0$

The effectiveness factor

$$\xi = \frac{1}{\varphi}\frac{3\varphi\coth(3\varphi) - 1}{3\varphi} \tag{7}$$

The Thiele modulus

$$\varphi = \frac{r_{\mathrm{Agg}}}{2}\sqrt{\frac{k_T/(1-\varepsilon_0^{\mathrm{CL}})}{D^{\mathrm{N}}_{\mathrm{O}_2,\mathrm{eff}}}} \tag{8}$$

In the anode, protons are produced and transported through the membrane to the catalyst layer. The flux expression of charges in the membrane and catalyst layer is

$$i_{\mathrm{p}} = -\kappa_{\mathrm{N,eff}}\nabla\phi \tag{9}$$

Liquid water flow in the porous media obeys Darcy's law. Its driving force is only the capillary force and the flow is similar to that used by Natarajan and Van Nguyen [18]. Liquid water permeability dependence on the saturation level is linear.

$$N_{\mathrm{w}} = -\frac{\rho_{\mathrm{w}}K_{\mathrm{w},0}}{M_{\mathrm{w}}\mu_{\mathrm{w}}}\left(-\frac{\mathrm{d}p_{\mathrm{c}}}{\mathrm{d}s}\right)s\nabla s \tag{10}$$

ρ_{w}, M_{w} and μ_{w} are the density, molecular weight, and viscosity of liquid water, respectively. $K_{\mathrm{w},0}$ is the permeability of liquid water at 100% saturation level. $-(\mathrm{d}p_{\mathrm{c}}/\mathrm{d}s)$ is treated as a constant, but the values used at GDL and CL are different.

In the GDL and CL, liquid water diffuses in the Nafion phase. In the membrane, liquid water transport is due to the water concentration gradient and electro-osmotic drag and similar to that considered by Lin et al. [19]:

$$N^{\mathrm{N}}_{\mathrm{w}} = \frac{n^{\mathrm{CL}}_{\mathrm{d}}}{F}i_{\mathrm{p}} - D^{\mathrm{N}}_{\mathrm{w}}\nabla C^{\mathrm{N}}_{\mathrm{w}} \tag{11}$$

Initially, all variables are zero except for the liquid water concentration in the Nafion phase, which is assumed to be in equilibrium with vapor water in the gas phase. All boundary conditions are listed in Table 2.

The governing equations and boundary conditions are discretized by the finite difference method. The convergence criteria for iteration and steady state are:

$$\left|\frac{V_i^{\mathrm{new}} - V_i^{\mathrm{old}}}{V_i^{\mathrm{old}}}\right| \le 1\times10^{-4} \tag{12}$$

V is an arbitrary variable.

3. Results and discussion

The parametric study for a two-phase, PEMFC cathode transient model is presented. The parameters used in this study are listed in Table 3.

The evolution of the *I–V* polarization curves are shown in Fig. 2. When the cell voltage is lower, for instance, $V_{\mathrm{s}} = 0.2$ V, and the current density overshoots with time due to the rapid electrochemical reactions. But when the cell voltage is higher, for instance, $V_{\mathrm{s}} = 0.6$ V, there is almost no overshoot.

Fig. 3 shows the saturation level distribution evolution with $V_{\mathrm{s}} = 0.2$, 0.4, and 0.6 V, respectively, since there is no water in the gas diffusion layer and the catalyst layer in the beginning. After start-up, liquid water is generated by electrochemical reactions in the catalyst layer and then diffuses to the gas diffusion layer. The liquid water saturation level accumulates until the steady state is reached. The generated liquid water will begin to affect the system after 1 s. Thus, the liquid water saturation level in the catalyst layer is higher than in the gas diffusion layer.

When the cell voltage is higher, for instance $V_{\mathrm{s}} = 0.6$ V, the electrochemical reaction is moderate and less liquid water is generated. Thus, the liquid water saturation level is lower than when a higher cell voltage is applied. When the cell voltage is lower, more liquid water is generated and begins to occupy the pores. The catalyst pellets surface have less oxygen, causing a decreased cell performance and a mass transport limitation.

Table 3
Parameters used in simulation

Gas diffusion layer properties	
Porosity	0.3
Thickness	0.025 cm
Permeability	10^{-9} cm^2
$-(\mathrm{d}p_{\mathrm{c}}/\mathrm{d}s)$	284.2 Dyne cm^{-2}
Catalyst layer properties	
Porosity	0.06
Thickness	0.0016 cm
Permeability	3×10^{-11} cm^2
$-(\mathrm{d}p_{\mathrm{c}}/\mathrm{d}s)$	568.4 Dyne cm^{-2}
Catalyst loading (m_{Pt})	0.4
Specific surface area of Pt (a_{Pt})	1000 cm^2 (mg Pt)$^{-1}$
Volumetric fraction of Nafion in catalyst pellet ($\varepsilon^{\mathrm{P}}_{\mathrm{N}}$)	0.393
Radius of catalyst pellet (r_{Agg})	10^{-5} cm
Thickness of Nafion	10^{-6} cm
Exchange current density ($i_{0,\mathrm{ref}}$ 0 °C)	10^{-6} A cm^{-2}
Membrane properties	
Thickness	0.005 cm
Porosity	0.35
Fixed charge site concentration	1.2×10^{-3} mol cm^{-3}
Operation conditions	
Temperature	60 °C
Pressure	1 atm
Mole fraction of oxygen in the air let	0.206
Humidity in air inlet	10%
Humidity at anode	100%

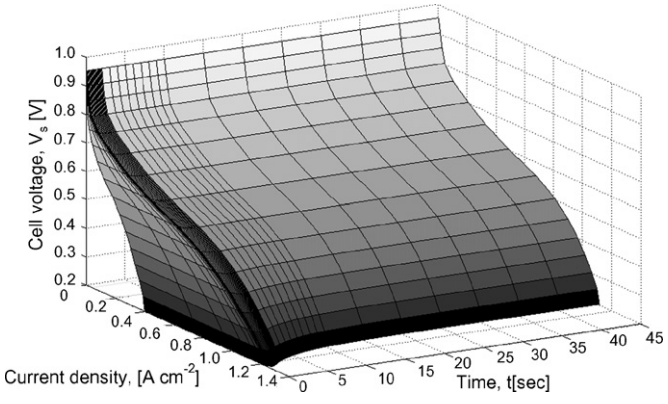

Fig. 2. The evolution profile of polarization curves.

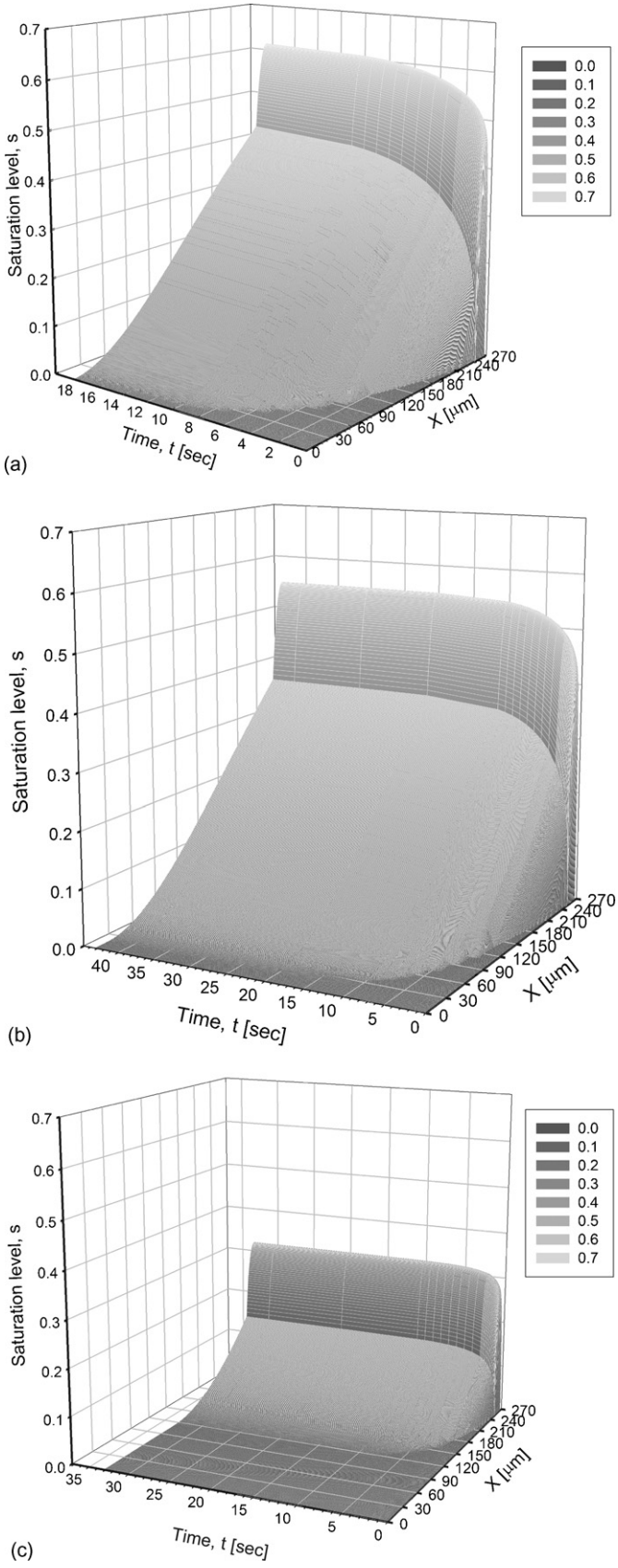

Fig. 3. The evolution profile of saturation level (base case): (a) $V_s = 0.2$ V, (b) $V_s = 0.4$ V, (c) $V_s = 0.6$ V.

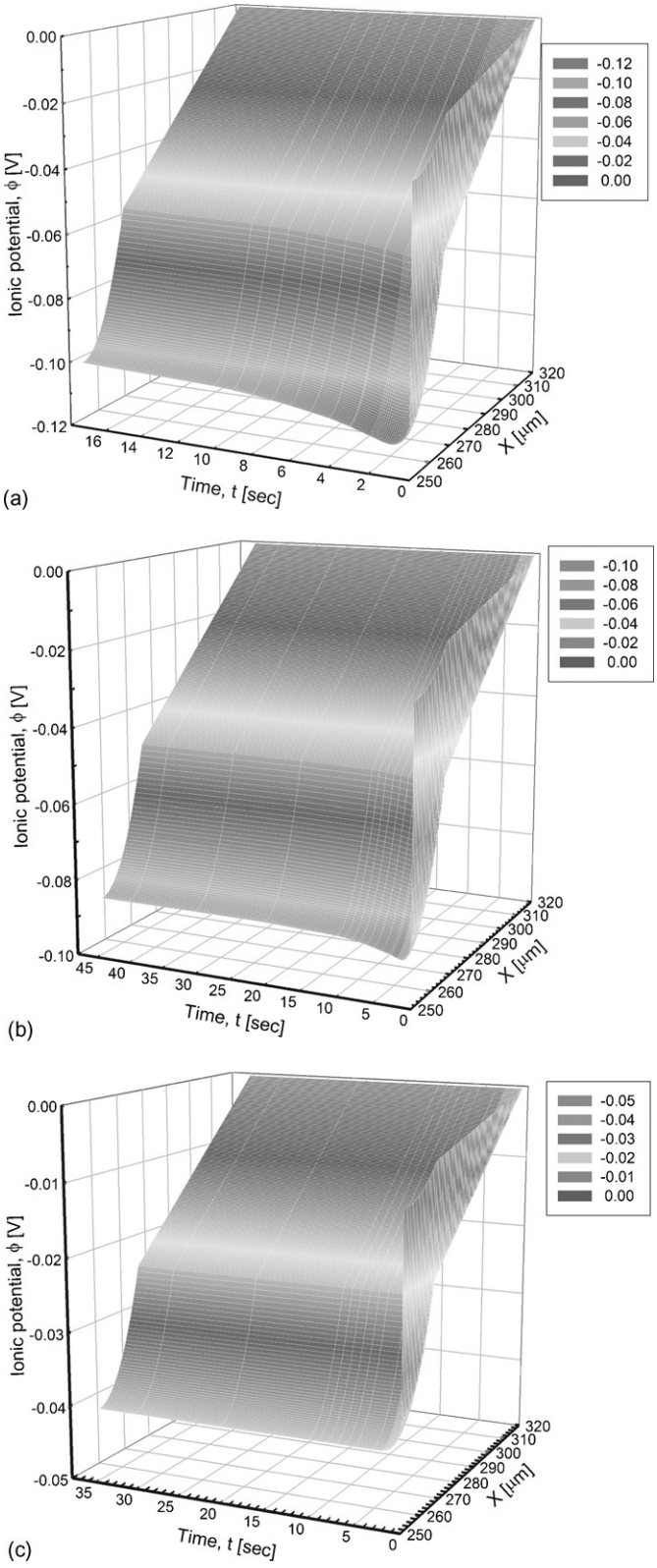

Fig. 4. The evolution profile of the ionic potential $\varepsilon_{CL} = 0.1$: (a) $V_s = 0.2$ V, (b) $V_s = 0.4$ V, (c) $V_s = 0.6$ V.

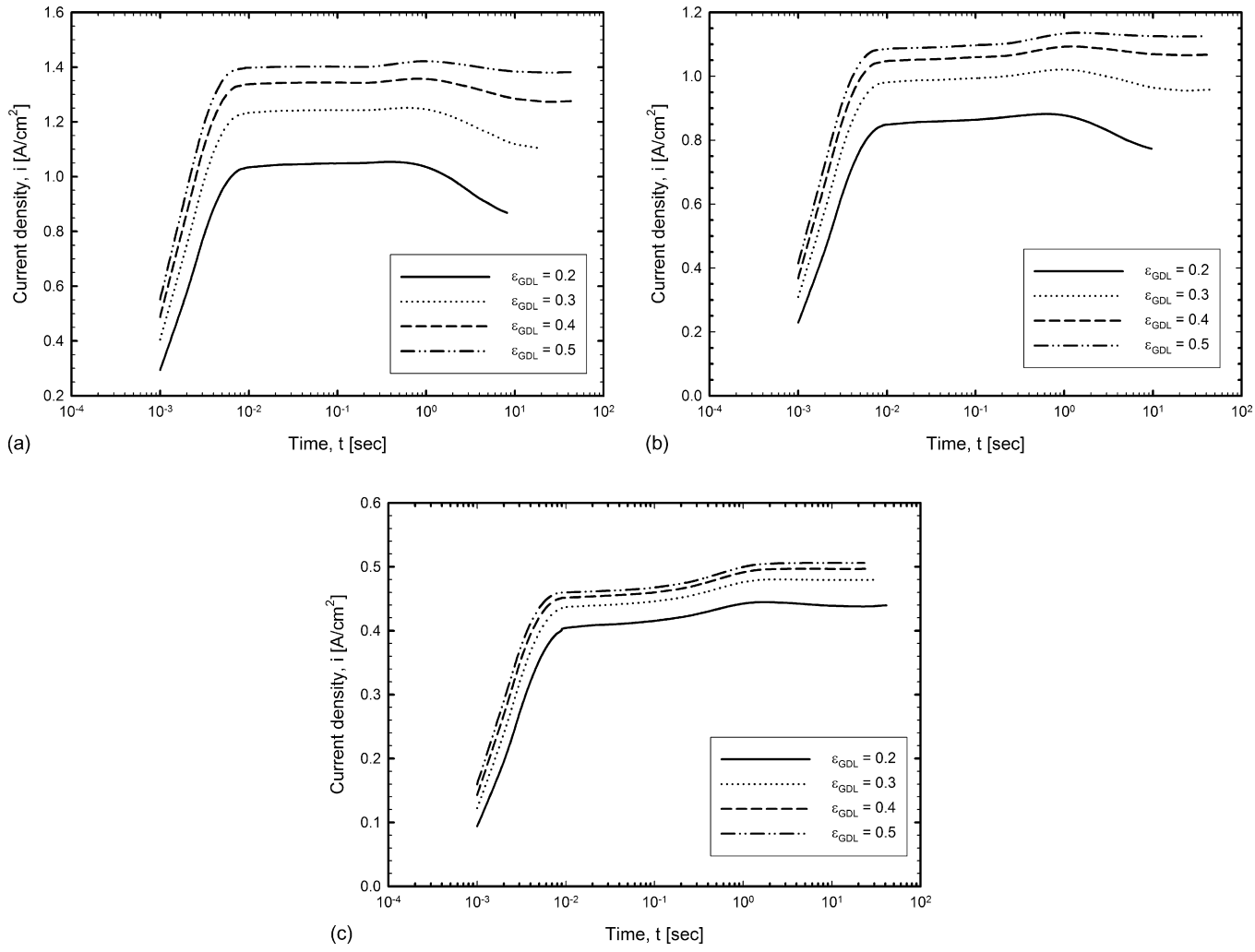

Fig. 5. The evolution profiles of current density with various gas diffusion layer porosity: (a) $V_s = 0.2$ V, (b) $V_s = 0.4$ V, (c) $V_s = 0.6$ V.

Fig. 4 shows the evolution of the ionic potential distribution with $V_s = 0.2$, 0.4, and 0.6 V, respectively. In the membrane, the ionic potential distribution shape is a straight line due to the absence of electrochemical reactions. In the catalyst layer, ionic potential distribution is nonlinear because of the electrochemical reactions.

When the cell voltage is higher, i.e., when the current density is smaller, the oxygen reduction reaction and the ionic potential loss are both smaller (Fig. 4c). When the cell voltage is lower, i.e., the current density is higher, the oxygen reduction reaction and the ionic potential loss are both larger (Fig. 4a). The present study shows several phenomena for the first time.

(1) Firstly, the variation of the ionic potential loss reaches a critical value, decreasing to a steady state, and is not monotonic.
(2) The ionic potential reaches 80% of its critical value in 0.005 s.
(3) The difference between the critical value and steady state of any given ionic potential is dependent on cell voltage applied. When cell voltage is 0.2 V, the difference is about 20%.

For a different GDL porosity, the cell current density curves, with $V_s = 0.2$, 0.4, 0.6 V, respectively, are shown in Fig. 5. Within 10^{-2} s, the current density rapidly rises. Between 10^{-2} and 10^{-1} s, the current density remains constant. But after 1 s, the

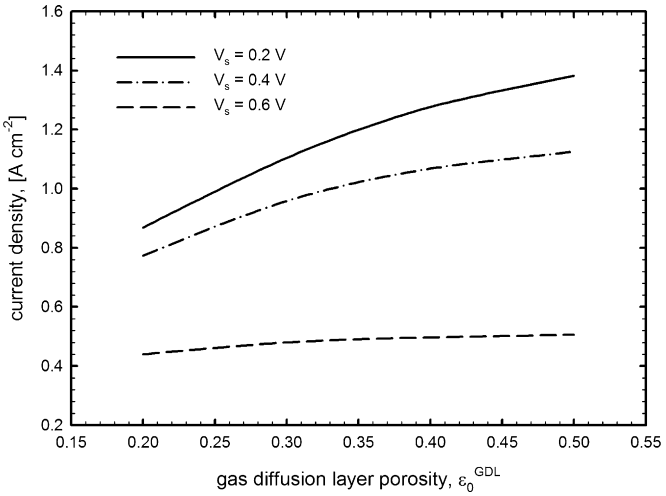

Fig. 6. Effect of GDL porosity porosity under various cell voltages in the steady state.

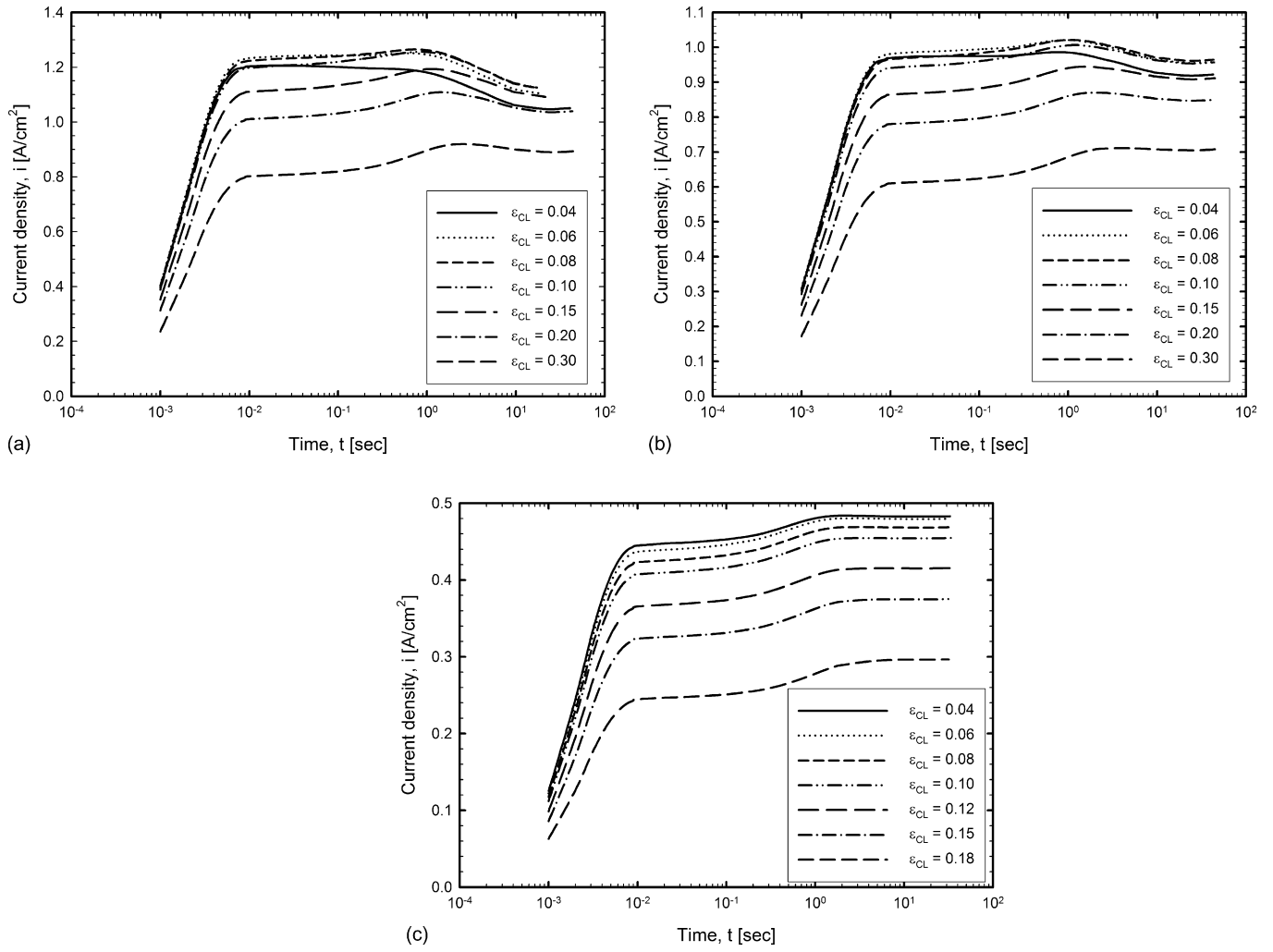

Fig. 7. The evolution profiles of current density with various catalyst layer porosity: (a) $V_s = 0.2$ V, (b) $V_s = 0.4$ V, (c) $V_s = 0.6$ V.

current density changes again. More liquid water accumulates after 1 s, as shown in Fig. 2. When $\varepsilon_{GDL} = 0.2$ and $\varepsilon_{GDL} = 0.3$, the current density drops, caused by liquid water hindrance on the oxygen transport due to reduced GDL porosity. When $\varepsilon_{GDL} = 0.4$ and $\varepsilon_{GDL} = 0.5$, the current density decreases slightly. This is because the GDL porosity is larger, so that liquid water hindrance on the oxygen transport is negligible. When $V_s = 0.6$ V, there is no liquid water effect and the current density remains constant. When $\varepsilon_{GDL} = 0.5$, a maximum current density is obtained.

On reaching steady state, the GDL porosity and the cell current density effects are shown in Fig. 6. Under the same cell voltage, between $\varepsilon_{GDL} = 0.2$ and $\varepsilon_{GDL} = 0.5$, gas diffusion layer porosity increases with current density. When the cell voltage is lower (Fig. 2), the liquid water effect is obvious. When $V_s = 0.2$ V, the current density difference between $\varepsilon_{GDL} = 0.2$ and $\varepsilon_{GDL} = 0.5$ is more than 40%, and when $V_s = 0.6$ V, the current density difference between $\varepsilon_{GDL} = 0.2$ and $\varepsilon_{GDL} = 0.5$ is small.

For a different CL porosity, the cell current density curves, with $V_s = 0.2$, 0.4, and 0.6 V, respectively, are shown in Fig. 7. When the CL porosity is higher, the catalyst loading, electrochemical reactions and the current density all decrease. When $\varepsilon_{CL} > 0.15$, the current density is lower. But a too small CL porosity causes the liquid water effect, the same as for lower GDL porosity. Furthermore, when $\varepsilon_{CL} = 0.04$, water flooding occurs even at 10^{-2} s and when $V_s = 0.6$ V, there is no liquid water effect. The current density increases with CL porosity.

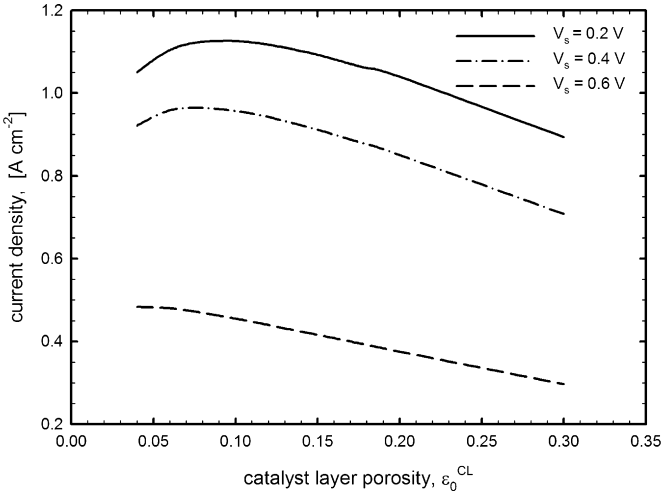

Fig. 8. Effect of CL porosity under various cell voltages in the steady state.

On achieving steady state, the CL porosity and the cell current density effect are shown in Fig. 8 from which it is clear that, when $V_s = 0.2$, 0.4 V, the optimum current density appears between $\varepsilon_{CL} = 0.06$ and $\varepsilon_{CL} = 0.10$.

4. Conclusion

A parametric two-phase, one-dimensional transient model of a proton exchange membrane cathode is the basis for this study. The model is developed to investigate the transient transport of gaseous species, protons and liquid water.

Firstly, the variation of the ionic potential loss reaches a critical value, decreasing to a steady state, and is not monotonic. This phenomenon is particularly obvious at lower cell voltages.

The current density rapidly rises within 10^{-2} s and remains constant between 10^{-2} and 10^{-1} s. But after 1 s, the current density is affected by the cell voltage, the catalyst layer porosity, and the gas diffusion layer porosity. When the cell voltage is higher, the electrochemical reactions are moderate, with no liquid water effects. But at lower cell voltages there are rapid electrochemical reactions and a liquid water effect. When $V_s < 0.4$ V, the liquid water effect should be taken into consideration.

For the gas diffusion layer porosity, the current density drops when $\varepsilon_{GDL} < 0.4$. This is caused by liquid water hindrance on the oxygen transport process because the GDL porosity is smaller. When $\varepsilon_{GDL} = 0.5$, the liquid water effect is small.

For catalyst layer porosity, when $\varepsilon_{CL} < 0.1$ the liquid water effect is obvious, but when $\varepsilon_{CL} > 0.1$, the liquid water effect not very apparent. When there is not enough catalyst to participate in the electrochemical reactions, the current density goes down. From these results, an optimum value appears between $\varepsilon_{CL} = 0.06$ and $\varepsilon_{CL} = 0.1$.

Acknowledgements

The authors would like to express appreciation to Professor Falin Chen, Chyi-Yeou Soong, Wei-Mon Yan, and Chih-Hsiang Cheng for their valuable comments. The National Science Council, Republic of China, supported this study through grant numbers NSC 93-2212-E-009-001.

References

[1] D.M. Bernardi, M.W. Verbrugge, J. Electrochem. Soc. 139 (1992) 2477–2491.
[2] D.M. Bernardi, M.W. Verbrugge, AIChE J. 37 (1991) 1151–1163.
[3] T.E. Springer, T.A. Zawodzinski, S. Gottesfeld, J. Electrochem. Soc. 138 (1991) 2334–2342.
[4] Y.W. Rho, S. Srinivasan, Y.T. Kho, J. Electrochem. Soc. 141 (1994) 2089–2096.
[5] N.P. Siegel, M.W. Ellis, D.J. Nelson, M.R. von Spakovsky, J. Power Sources 128 (2004) 173–184.
[6] W. Sun, B.A. Peppley, K. Karan, J. Power Sources 144 (2005) 42–53.
[7] W. Sun, B.A. Peppley, K. Karan, Electrochim. Acta 50 (2005) 3359–3374.
[8] F. Jaouen, G. Lindbergh, G. Sundholm, J. Electrochem. Soc. 149 (2002) A437–A447.
[9] N.P. Siegel, M.W. Ellis, D.J. Nelson, M.R. von Spakovsky, J. Power Sources 115 (2003) 81–89.
[10] K.M. Yin, J. Electrochem. Soc. 152 (2005) A583–A593.
[11] K. Broka, P. Ekdunge, J. Appl. Electrochem. 27 (1997) 281–289.
[12] Y. Bultel, P. Ozil, R. Durand, Electrochim. Acta 43 (1998) 1077–1087.
[13] Y. Bultel, P. Ozil, R. Durand, J. Appl. Electrochem. 30 (2000) 1369–1376.
[14] F. Gloaguen, P. Convert, S. Gamburzev, O.A. Velev, S. Srinivasan, Electrochim. Acta 43 (1998) 3767–3772.
[15] T. Berning, N. Djilali, J. Electrochem. Soc. 150 (2003) A1589–A1598.
[16] W.S. He, J.S. Yi, T. Van Nguyen, AIChE J. 46 (2000) 2053–2064.
[17] D. Natarajan, T. Van Nguyen, J. Electrochem. Soc. 148 (2001) A1324–A1335.
[18] D. Natarajan, T. Van Nguyen, J. Power Sources 115 (2003) 66–80.
[19] G.Y. Lin, W.S. He, T. Van Nguyen, J. Electrochem. Soc. 151 (2004) A1999–A2006.
[20] T.E. Springer, M.S. Wilson, S. Gottesfeld, J. Electrochem. Soc. 140 (1993) 3513–3526.
[21] R.B. Bird, W.E. Stewart, E.N. Lightfoot, Transport Phenomena, Wiley, New York, 1960.